L-shell ionization of Cd: Structure of the x-ray emission spectrum

F. Fernandez [a,b], A. Sepúlveda [c], J. Trincavelli [a,b], G. Castellano [a,b,*]

[a] *Universidad Nacional de Córdoba, Facultad de Matemática, Astronomía, Física y Computación, Medina Allende s/n, Ciudad Universitaria (5000) Córdoba, Argentina*
[b] *Instituto de Física Enrique Gaviola (IFEG), CONICET, Medina Allende s/n, Ciudad Universitaria (5000) Córdoba, Argentina*
[c] *Facultad de Ciencias Naturales, Matemática y del Medio Ambiente, Universidad Tecnológica Metropolitana, Santiago, Chile*

ARTICLE INFO

ABSTRACT

The cadmium L x-ray spectrum induced by electron impact was analyzed in detail. The measurements were performed on a bulk pure sample using a commercial wavelength dispersive spectrometer, and the spectrum was processed with a parameter optimization method previously developed. This procedure permitted the determination of characteristic energies, relative transition probabilities and natural linewidths for this element. The results obtained here were compared to the data found in the literature, when available. Spectral structures related to satellite and radiative Auger Effect emissions were also analyzed, assessing energy shifts and relative intensities. Some of these parameters were determined for the first time, even in overlapping peaks and weak transitions, which was possible due to the robustness of the spectral processing method used.

1. Introduction

The study of X-ray emission in atomic transitions is very useful in the field of atomic physics, for example, to test theoretical models and some approximations assumed in them [1,2]. In fact, a good knowledge of the structure of X-ray emission spectra is key to give a detailed description of the fundamental processes that govern the interaction of electrons with matter. On the other hand, the X-ray emission associated with inner shell transitions contains useful information about the atomic structure, and also about several molecular and solid-state effects. A detailed study of the X-ray emission involving decays originated in inner-shell hole atomic states is therefore essential for a better understanding of the different processes that can take place as relaxation mechanisms.

In addition, an adequate set of experimental data for fundamental parameters, such as characteristic energies, relative transition probabilities (RTP), natural linewidths (Γ), satellite lines and radiative Auger emission (RAE), becomes crucial for several spectroscopic techniques based on X-ray emission, since peak overlaps between different lines of neighboring elements are frequently a problem for the analyst.

The specific case of the cadmium L spectrum is of particular interest due to the scarcity of data available in the literature. An adequate knowledge about the fundamental parameters mentioned is useful to solve problems in the deconvolution of the Cd-L spectrum inherent in analytical techniques such as electron probe microanalysis, X-ray fluorescence or particle induced X-ray emission. At present, the relevance of the capability for the determination of cadmium arises, on one hand, from its important industrial applications on electric batteries, pigments [3], coatings [4], and electroplating [5], and on the other hand, from its high toxicity [6,7], which implies the necessity of continuously monitoring this element as environmental pollutant to a high degree of sensitivity. The increased emissions resulting from its production, use, and disposal, combined with its persistence in the environment, and its relatively rapid uptake and accumulation by food chain crops contribute to its potential environmental hazards. Cadmium may find its way to the human population through food and beverage, drinking water, air, and cigarette smoking; although respiratory intoxication by cadmium is rare, acute cases may still be occasionally observed [8]. Among the commercial fertilizers, those involving phosphorus contain somewhat elevated levels of Cd; it has been shown that the long-term use of phosphorus fertilizers slightly increases the concentration of Cd in surface soils [9]. For these reasons, monitoring Cd level in soils should be a routine strategy in food production, and the detailed knowledge of Cd L-lines is necessary to prevent a miscalculation of Cd concentrations induced by spectral interference with other elements. Particularly, there is a strong overlapping of Cd-Lβ_1 and K-Kα, which could lead to wrong analysis, since potassium is usually the second most abundant of the major nutrient elements in soil, only below nitrogen. The total K content of soils varies from < 0.01% to about 4% and is commonly about 1% [10].

Cd is surveyed through X-ray analyses in food and biological samples, environmental studies involving airborne particulates, soils, water from various sources, and materials and technological applications. Although the present work focuses on electron beam irradiation, the fundamental parameters investigated are obviously applicable to any technique based on X-ray emission. To experimentally obtain these parameters, the measured spectra must be processed by means of a reliable method, since all spectral contributions must be appropriately taken into account: characteristic peaks, bremsstrahlung continuum, satellite bands and RAE structures, as well as detection artifacts.

Experimental characteristic energies have been reported by Bearden [11] and Cauchois and Sénémaud [12] for many elements, including cadmium. On the other hand, Deslattes et al. [2] performed theoretical calculations for K and L diagram energies, considering also prohibited transitions and other lines not observed experimentally. Regarding RTPs, these parameters were predicted by Perkins et al. [13] for all elements and transitions. In addition, natural linewidths have been scarcely investigated despite their usefulness [14]; a set for these data was compiled by Campbell and Papp [15] for a large number of transitions, whereas some measurements were made by Ohno et al. [16].

The aim of this work is to analyze the structure of the L X-ray spectrum induced by electron impact for cadmium. The experimental data acquired evidenced 16 diagram transitions to L-shell vacancy states for this element. For all them, the characteristic energies and relative transition probabilities were determined, with the exception of the $L\alpha_1$ emission, whose characteristic energy was taken as reference (see below). In addition, most natural linewidths were obtained, multiple ionization satellite lines and RAE bands being also studied. To this end, the experimental spectrum was processed taking into account all the mentioned contributions, by means of a robust fitting procedure based on a method implemented previously to refine atomic and instrumental parameters [17].

2. Experimental

The L-spectrum from a pure bulk Cd sample was acquired with a JEOL JXA 8230 microprobe, equipped with a Johansson type wavelength dispersive spectrometer (WDS). The emitted X-rays were diffracted by a PET analyzing crystal, whose efficiency curve $\varepsilon(E)$ as a function of the detected photon energy E was previously characterized [18], and recorded by a P10 flow counter. Although the purity extent of the cadmium standard needs not to be extremely high, a careful survey has been performed to check for possible interferences from eventual impurities; this was carried out along a wavelength range large enough to include all the emission energies involved. The emission spectrum was induced by a 10 keV incident electron beam, and collected at a take-off angle of 40°. The beam current was set to 11 nA, as registered by the instrument built-in probe current detector, accumulating 4 spectra with 1213 spectrometer positions each, acquiring 3.0 s in each position. These settings were adequate to achieve good statistics in the resulting spectrum, obtained by the summation of the four spectra acquired, and enabled to appropriately discriminate most low intensity lines.

3. Spectral analysis

The resulting spectrum obtained was processed by means of the software POEMA [17], which relies on the numerical optimization of atomic and experimental parameters. Through this procedure, an analytical expression is optimized to best match the measured intensities I_i recorded at channel i. This expression provides a description for the intensity $\bar{I}_i$ as a function of the bin energies E_i of the acquisition system

$$\bar{I}_i = B(E_i) + \sum_q P_q S_q(E_i), \tag{1}$$

where B accounts for the background radiation and S_q models the peak profile [19] corresponding to the line intensity P_q. The model used for the bremsstrahlung spectrum $B(E_i)$ emerging form the sample is taken from Ref. [20]. The shaping choices for each peak profile are detailed below, whereas the number of photons P_q associated with the q emission is assessed as

$$P_q = \beta \sigma_\ell^x p_q (ZAF)_q \, \varepsilon(E_q), \tag{2}$$

where β is proportional to the number of incident electrons, σ_ℓ^x is the ℓ subshell X-ray production cross section, *i.e.*, the total vacancy production cross section $\tilde{Q}_\ell$ multiplied by the fluorescence yield ω_ℓ; p_q is the corresponding radiative transition rate and the factors Z, A and F are respectively the atomic number, absorption and fluorescence matrix correction factors. In the peaks analyzed in this work, A could be considered uniform within the narrow energy interval involved in the linewidth; in certain cases, however, the dependence of A on the photon energy must be carefully taken into account, even within one linewidth, as explained and implemented in a previous work [18].

The total vacancy production cross sections for each L-shell can be written as

$$\tilde{Q}_{L_1} = Q_{L_1},$$
$$\tilde{Q}_{L_2} = Q_{L_2} + f_{1,2} Q_{L_1},$$
$$\tilde{Q}_{L_3} = Q_{L_3} + f_{2,3} Q_{L_2} + (f_{1,3} + f_{1,2} f_{2,3}) Q_{L_1},$$

where Q_ℓ is the ionization cross section for the ℓ subshell and $f_{k,j}$ represents the Coster–Kronig probability for a transition from an initial L_k subshell vacancy state to a final L_j subshell vacancy state.

The fitting procedure involves the minimization of quadratic differences between the experimental spectrum I_i and the one estimated by Eq. (1), by means of the refinement of the parameters intervening in the assessment of the intensities $\bar{I}_i$. The estimator to minimize is then

$$\chi^2 = \frac{1}{N_c - N_p} \sum_{i=1}^{N_c} \frac{(\bar{I}_i - I_i)^2}{\bar{I}_i},$$

where N_c is the number of channels for the region of interest in the spectrum to analyze, and N_p is the number of optimized parameters. After several optimization steps, an appropriate spectrum characterization is reached, which implies the determination of the atomic and instrumental parameters allowed to vary. The uncertainties associated with each magnitude determined by means of the optimization process are estimated by applying the law of propagation of uncertainties, from the statistical uncertainty inherent to each experimental intensity I_i. This assessment is carried out through a numerical differentiation of the analytical spectrum with respect to the sought parameters [21].

It is worth pointing out that often a spectral fit improves by artificially increasing the number of structures taken into account. The strategy followed along this work aimed always to keep the minimum number of peaks producing a reasonable fit. X-ray spectra from pure elements with atomic numbers close to cadmium (ruthenium, silver and tellurium) were characterized previously [22], those previous results being quite helpful to make decisions related to the lines included in the analysis of this element. In the present work, whenever a transition not previously reported in the literature was introduced, it was clear that the presence of this emission in the spectrum was evident, which became manifest in a dramatical worsening of the fitting when this line was omitted.

To describe the profiles for the diagram lines, a Voigt function was chosen in this work, which is a convolution of two probability distributions, a Gaussian $G(E)$ related to the instrumental features, and a Lorentzian $L_q(E)$ whose width is related to the average lifetime of the initial vacancy status [23]

$$S_q(E) = \int L_q(E') \, G(E - E') dE'. \tag{3}$$

A Gaussian profile was chosen to model the satellite lines, since this function results more adequate to describe the joint effect of the
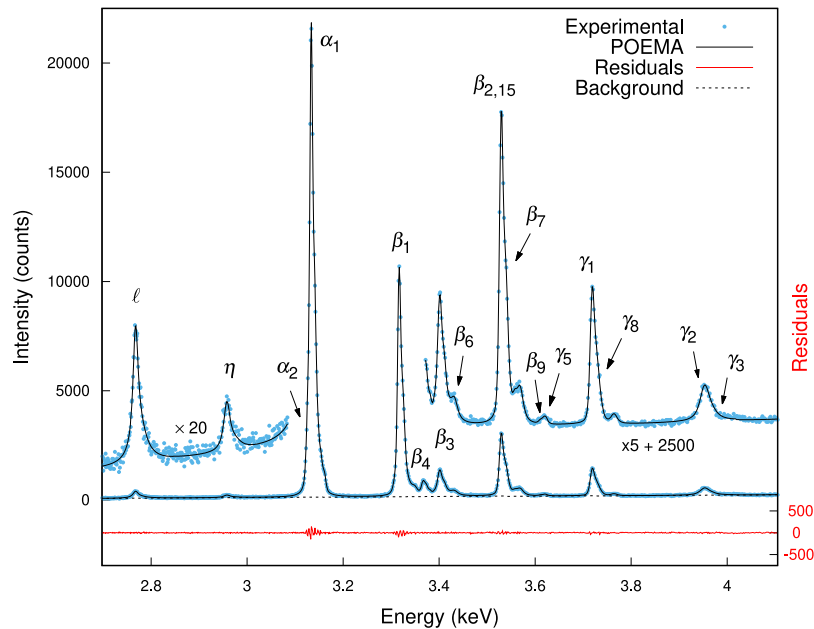
Fig. 1. Cd L-spectrum measured at 10 keV. The insets show magnified views of the regions involving weak peaks. Only diagram lines have been labeled (more detail for satellite lines is given below).

numerous non-diagram transitions responsible for each of the satellite structures included. Instead, in order to take into account the asymmetric shape of the RAE structures, an expression involving the convolution of a Gaussian profile and the profile suggested by Enkisch et al. [24] was implemented.

4. Results and discussion

Fig. 1 displays the measured and predicted Cd L-spectra, along with the corresponding residuals. In the global fitting process, a good agreement has been achieved, with a χ^2 value of 1.22. All the peaks observed were identified in this plot as diagram lines, correspondingly labeled with their respective name, and the structures around them as satellite lines and RAE bands. In the following sections, details about the data obtained for the atomic parameters involved are discussed.

Special care has been taken in the estimation of uncertainties, to properly take into account parameters not strongly correlated, since the formalism mentioned for uncertainty propagation assumes that the set of refined parameters may be regarded as a set of independent stochastic variables. In those cases in which a strong correlation between some parameters was observed, new optimization steps were performed by avoiding the presence of pairs of these correlated magnitudes. This was the case, for instance, of the L_3N_1 (β_6) characteristic energy and the L_2M_4 (β_1) natural linewidth, whose strong correlation prevented the assessment of uncertainties from their joint optimization. To achieve a more realistic estimate of this energy uncertainty, it was necessary to keep the mentioned linewidth fixed (and vice versa), even when both parameters were optimized simultaneously for the determination of their magnitudes.

4.1. Characteristic energies

The $L\alpha_1$ emission energy given by Bearden [11] for pure Cd (3.13373 keV) was used as reference for the spectrometer calibration procedure [25]. In order to validate this calibration routine, which was finally used in the whole optimization process, all other characteristic energies obtained in this work were compared with those published by Bearden [11], Cauchois and Sénémaud [12] and Deslattes et al. [2], as displayed in Table 1. To estimate the uncertainty of each transition

Table 1
Characteristic energies (in keV) obtained for Cd. Numbers in parentheses indicate the estimated uncertainties in the last digits.

Transition	This work	Ref. [11]	Ref. [12]	Ref. [2]
L_3M_1 (ℓ)	2.7638(2)	2.76735	2.76732	2.7679(14)
L_3M_4 (α_2)	3.1261(8)	3.12691	3.12688	3.1275(10)
L_3N_1 (β_6)	3.435(1)	3.42994	3.42996	3.4312(34)
L_3N_4 (β_{15})	3.5291(1)	3.52812	3.5282	3.52742(79)
L_3N_5 (β_2)				3.52874(97)
L_3O_1 (β_7)	3.5383(4)	–	–	–
L_2M_1 (η)	2.9572(8)	2.95675	2.95675	2.9571(12)
L_2M_4 (β_1)	3.3169(1)	3.31657	3.31660	3.3167(11)
L_2N_1 (γ_5)	3.620(1)	3.61935	3.6193	3.6204(35)
L_2N_4 (γ_1)	3.7189(2)	3.71686	3.7168	3.71667(85)
L_2O_1 (γ_8)	3.7294(4)	–	–	–
L_1M_2 (β_4)	3.368(1)	3.36719	3.36727	3.3669(21)
L_1M_3 (β_3)	3.4016(2)	3.40145	3.40148	3.4006(19)
L_1M_5 (β_9)	3.608(5)	3.61445	3.6144	3.6133(16)
L_1N_2 (γ_2)	3.950(1)	3.9513	3.9514	3.9496(41)
L_1N_3 (γ_3)	3.962(2)			3.9490(22)

energy, the fitting uncertainty was added in quadrature with that reported by Bearden for the line taken as reference.

When comparing the present results with Ref. [11] and Ref. [12], the doublet $L_1N_{2,3}$ was not resolved by these authors; to perform the comparison in this case, a weighted average energy was assessed for the involved decays, with the corresponding relative transition probabilities p_q reported in this work (see Section 4.2)

$$E = \frac{p_1 \cdot E_1 + p_2 \cdot E_2}{p_1 + p_2}, \qquad (4)$$

where p_q and the emission energies E_q are associated to the corresponding transition q. The same assessment was carried out for the energies reported by Deslattes et al. [2], also using the RTPs obtained in this work. On the other hand, the $L\beta_{2,15}$ doublet could not be resolved in the present assessment, as well as in Ref. [11] and Ref. [12]; the comparison with the separated energies given by Deslattes et al. [2] was performed by using Eq. (4) with the RTPs given by Perkins et al. [13].

The comparison between the characteristic energies obtained in this work and those found in the literature is displayed in Fig. 2. With a few exceptions, the differences are below 2.5 eV. The largest disagreements
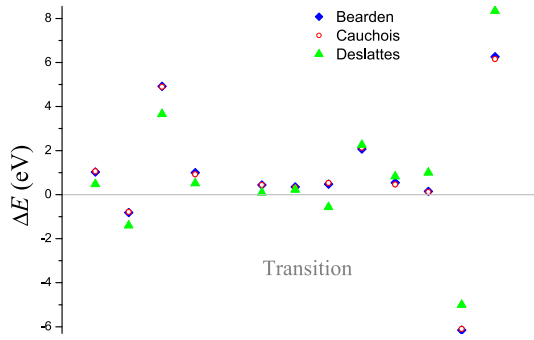
Fig. 2. Differences of the characteristic energies obtained in this work relative to those reported by other authors. The order of the transitions represented on the abscissas is the same as in Table 1 —excepting L_3M_5 (taken as reference) and the lines not reported before, i.e., L_3O_1 and L_3O_1. Squares: Ref. [11], open circles: Ref. [12], triangles: Ref. [2].

Table 2
Relative transition probabilities obtained along this work. Numbers in parentheses indicate the estimated uncertainties in the last digits.

Transition	This work	Ref. [13]
L_3M_1 (ℓ)	0.041(1)	0.0980
L_3M_4 (α_2)	0.055(5)	0.0823
L_3M_5 (α_1)	0.802(7)	0.7306
L_3N_1 (β_6)	0.007(4)	0.0067
$L_3N_{4,5}$ ($\beta_{2,15}$)	0.053(3)	0.0819
L_3O_1 (β_7)	0.041(3)	0.0005
L_2M_1 (η)	0.031(3)	0.0596
L_2M_4 (β_1)	0.869(7)	0.8464
L_2N_1 (γ_5)	0.005(1)	0.0066
L_2N_4 (γ_1)	0.057(2)	0.0871
L_2O_1 (γ_8)	0.037(5)	0.0004
L_1M_2 (β_4)	0.303(7)	0.3163
L_1M_3 (β_3)	0.54(4)	0.5225
L_1M_5 (β_9)	0.007(4)	0.0055
L_1N_2 (γ_2)	0.077(8)	0.0583
L_1N_3 (γ_3)	0.069(8)	0.0975

Fig. 3. Differences of the RTP values obtained in this work relative to the data reported by Perkins et al. [13]. The transitions displayed on the abscissas run in the same order as in Table 2.

Table 3
Natural linewidths (in eV) obtained in this work. Numbers in parentheses indicate the estimated uncertainties in the last digits.

Trans.	This work	Ref. [15]	Ref. [16]
L_3M_1 (ℓ)	15.4(6)	11.04	11.9
L_3M_4 (α_2)	2.5(5)	2.58	–
L_3M_5 (α_1)	3.1(1)	2.59	–
L_3N_4 (β_{15})	2.3(2)	2.29	3.1
L_3N_5 (β_2)		2.29	
L_3O_1 (β_7)	8.4(7)	–	–
L_2M_1 (η)	15(2)	11.22	11
L_2M_4 (β_1)	3.3(1)	2.76	–
L_2N_1 (γ_5)	7(3)	6.82	–
L_2N_4 (γ_1)	2.7(3)	2.47	3.1
L_2O_1 (γ_8)	7(1)	–	–
L_1M_2 (β_4)	8(1)	6.05	–
L_1M_3 (β_3)	8(1)	6.30	–
L_1M_5 (β_9)	9(8)	3.85	–
L_1N_2 (γ_2)	13(2)	14.3	19.0
L_1N_3 (γ_3)	18(2)	14.0	

occur for the L_1M_5 (β_9) and $L_1N_{2,3}$ ($\gamma_{2,3}$) emissions. In the first case, the registered spectrum evidences a strong overlap of this extremely weak line on the low energy region of the more intense L_2N_1 (γ_5) peak, which obviously hampers an accurate fitting. In the case of the $L_1N_{2,3}$ ($\gamma_{2,3}$) doublet, it must be stressed that these lines were properly resolved along the present work, which is not the case in the data provided in other experimental observations. In addition, it is worth noticing that the values found for these lines maintain the relationship $E(\gamma_3) > E(\gamma_2)$, as observed for other elements —see for instance the elements with atomic numbers 47, 55 and 57 in Ref. [11]—, in contrast to the values reported in Ref. [2], which are indistinguishable among themselves.

4.2. Relative transition probabilities

Each RTP is defined as the relative probability for a transition corresponding to the L_kX_j emission normalized to all radiative decays to the L_k subshell. Table 2 displays the RTP values found in this work, along with the data given by Perkins et al. [13]. In the present assessment of these RTPs, the normalization was performed by taking into account only those transitions observed experimentally here.

Although the RTPs obtained in the present work do not show a close agreement with those reported in [13] (see Table 2 and also Fig. 3), it must be borne in mind that the latter do not originate in measurements, but rely on previous theoretical estimates and subsequent evaluations. It is important to stress that no previous experimental determination of this set of RTPs was reported before.

4.3. Natural linewidths

A diagram line is properly described by a Voigt profile, in which the emitted Lorentzian photon profile is convoluted with a Gaussian function with half width at half maximum γ_G associated to the instrumental broadening [22]. This spectrometer width γ_G is governed by the angular divergence $\Delta\theta$ of the crystal analyzer, and a lower bound for it can be derived from the Bragg's law, resulting in [23]

$$\gamma_G = \sqrt{2\ln 2}\; \Delta\theta\; E \sqrt{\left(\frac{2d}{hc}E\right)^2 - 1} \tag{5}$$

where d is the crystal interplanar spacing, h is the Planck constant and c is the speed of light in vacuum. Each peak with energy E is therefore described by two parameters that can be refined by POEMA: its natural linewidth and the angular divergence $\Delta\theta$ associated to the analyzing crystal —the latter being the same for all peaks in the spectrum.

Table 3 displays the natural linewidths obtained in this work along with experimental data published by Ohno et al. [16] and values calculated from the sum of the widths of those energy levels involved in each decay published by Campbell and Papp [15]. As can be seen, the results shown here are consistent with the values reported previously, except for the weak transitions L_3M_1 ($L\ell$) and L_1M_5 ($L\beta_9$) —the latter being overlapped with the L_2N_1 (γ_5) line, which hampers this linewidth characterization. Moreover, experimental natural linewidths corresponding to cadmium L_3O_1 ($L\beta_7$) and L_2O_1 ($L\gamma_8$) emissions are presented here for the first time. From this information, and taking into account that the widths associated to the L_3 and L_2 energy levels are respectively 2.24 eV and 2.38 eV [16], the energy width for the cadmium O_1 level can be estimated as (6 ± 1) eV.

Table 4
Relative energies and areas of satellite lines.

Parent line	ΔE (eV) This work	ΔE (eV) Ref. [12]	Relative area (%)
L_3M_1 (ℓ)	21(6)	–	13(2)
$L_3M_{4,5}$ (α)	7(2)	6.7	14.2(5)
	12(1)	14.7	8.0(3)
	20(1)	20.1	9.5(2)
	27(4)	26.9	0.91(9)
$L_3N_{4,5}$ ($\beta_{2,15}$)	29(6)	29.9	7.4(9)
	39(1)	34.7	17.3(9)
L_2M_1 (η)	14(4)	–	23(7)
L_2M_4 (β_1)	8.2(2)	9.0	16.3(4)
	14.6(6)	16.1	9.0(4)
	30.8(4)	30.6	3.7(3)
L_2N_4 (γ_1)	34(5)	37.2	6(1)
	48(1)	–	6.8(9)
L_1M_2 (β_4)	7.0(5)	–	8(1)
	14(1)	–	7.7(8)
	23(2)	–	2.8(8)
L_1M_3 (β_3)	10.5(4)	–	10.7(9)
	23(1)	–	10.5(9)

Table 5
Relative energies and areas of RAE bands.

Parent line	ΔE (eV)	Relative area (%)
L_3M_5 (α_1)	−7(2)	0.5(1)
L_2M_4 (β_1)	−10.7(9)	1.3(2)

4.4. Satellite lines and radiative auger emission

Different phenomena give rise to the X-ray emission associated to the multiple peak structures which appear in the experimental spectra. Among the events originating these structures are multiple ionizations, which can slightly distort the atomic energy levels, resulting in the so-called spectator hole satellite lines. Another possible relaxation mechanism of inner-shell vacancy states may lead to radiative Auger emissions, in which the final state is a doubly ionized atom accompanied by the emission of an outer electron and an X-ray photon [22].

The transitions, corresponding to spectator hole satellite lines, bear very close energies and cannot always be separately observed, due to the overlap originated in the natural linewidths involved, and also because of the limited spectrometer energy resolution. Their joint effect, however, can be phenomenologically modeled by incorporating a small number of satellite lines, the cause of them corresponding in fact to a mixture of different issues.

Tables 4 and 5 summarize the energy shifts and relative areas of the satellite lines and RAEs structures obtained. The energy shifts ΔE displayed were defined as the differences between the out-of-diagram line and that of the main decay to which it is associated. In the first table, data published by Cauchois and Sénémaud [12] are also included for comparison. Relative areas were calculated as the ratios of the corresponding peak area to the sum of the areas from the parent line and all the RAEs and satellites associated to it. In those cases where these emissions can be compared, it can be seen that most of the energies assigned to the satellite lines are in a quite good agreement with those reported by Cauchois and Sénémaud [12]. The results obtained here include satellite lines not previously reported, associated with the diagram lines L_3M_1, L_2M_1, L_2N_4, L_1M_2 and L_1M_3. Other satellite lines were reported in [12], not observed here perhaps because of their low intensity.

As explained elsewhere [22], the relaxation energy in an L_kR_j transition may be jointly released by the emission of a photon along with an Auger electron ejected from the T_k shell. In this decay the energy balance translates to

$$E(T_k) \lesssim E(L_kR_j) - E_m, \tag{6}$$
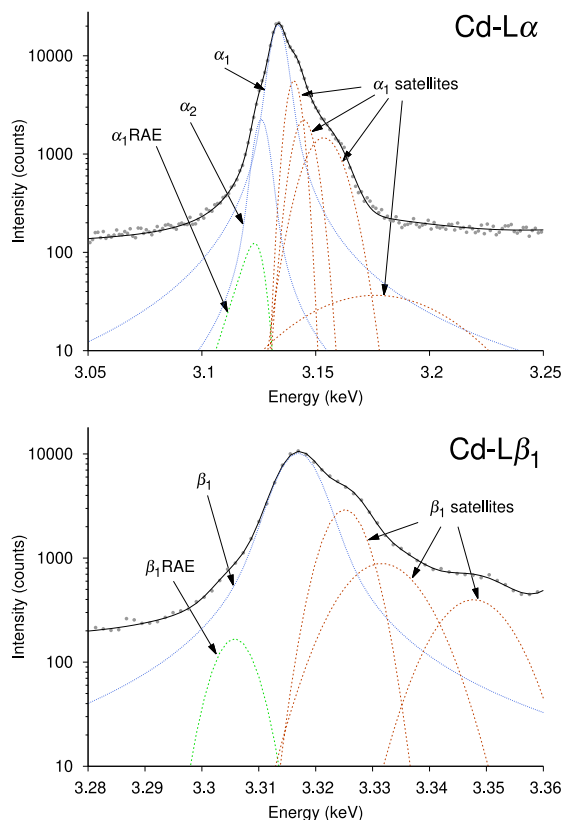
Fig. 4. X-ray spectrum of Cd in the Lα and Lβ_1 regions. Dots: experimental spectrum; solid line: spectral fitting; dashed line: contribution of each diagram, satellite and RAE transition.

where $E(T_k)$ is the Auger electron binding energy, $E(L_kR_j)$ stands for the characteristic energy associated to the L_kR_j transition, and E_m is the energy of the RAE band maximum. Thus, the energy difference ΔE displayed in Table 5 approximately corresponds to the binding energy of the Auger electron involved. A RAE structure obtained after processing a spectrum can be associated to some specific absorption edge on the basis of in Eq. (6). With this relationship in mind, both RAE bands observed here for Cd may be associated with the $N_{4,5}$ edge. Such identification arises from considering the values suggested by Larkins [26] and Bearden and Burr [27], who reported 9.3 eV for the $N_{4,5}$ absorption edge, which is the binding energy closest to the values displayed in Table 5. Fig. 4 shows the Cd Lα and Lβ_1 spectral regions, where the fitting curve, the contributions of the diagram lines, satellite lines and RAE structures are detailed. As can be seen, the final predictions for these spectral regions are very good.

5. Conclusion

After a careful study of the experimental Cd X-ray spectrum, 15 characteristic energies, 16 RTPs and 14 natural linewidths were obtained for the associated L emissions. In addition, several spectator hole satellite lines and RAE structures associated with the main lines were also investigated.

In most cases, the data obtained along this work for the characteristic energies are in good agreement with those found in the literature. The case of L_1N_2 and L_1N_3 lines may be highlighted, since previous experimental studies reported them as doublets, although in this work they were plainly resolved with the spectral processing routine used. In addition, these characteristic energies must be carefully considered in future assessments, since the results for them bear higher energies than those reported previously in the literature; it is worth noticing,

however, that the values found for these lines maintain the energy relationship $E(\gamma_3) > E(\gamma_2)$ observed in the general trend for other elements.

To the best of the authors' knowledge, no experimental data for L-shell RTPs have previously been reported for cadmium. The set of RTPs obtained here were therefore compared only with interpolations to theoretical calculations [13], showing certain global general agreement.

The values obtained here for the natural linewidths were compared with previous experimental data and those resulting from the addition of the energy level widths corresponding to the states involved in each transition. The reasonable agreement achieved in the majority of cases supports the reliability of the data obtained for L_2O_1 and L_3O_1 linewidths, for which no previous estimations were available.

The satellite line energies characterized along the present work were compared with the few values available in the literature; in addition, their relative areas were also evaluated. The study of the RAE profiles led to the characterization of some spectral structures that had not been previously studied; the corresponding energy, the relative area as compared to the parent line and the atomic level of the emitted Auger electron were also identified.

It is important to emphasize the importance of characterizing the L_2O_1 and L_3O_1 emissions, since their characteristic energies and corresponding transition rates were not experimentally determined before. The determination of their natural linewidths permitted to infer the energy width for the atomic cadmium O_1 level, also experimentally determined for the first time.

Declaration of competing interest

The authors declare that they have no known competing financial interests or personal relationships that could have appeared to influence the work reported in this paper.

Acknowledgments

References

[1] J.H. Scofield, Hartree-Fock values of L x-ray emission rates, Phys. Rev. A 10 (1974) 1507.

[2] R.D. Deslattes, E.G. Kessler Jr., P. Indelicato, L. de Billy, E. Lindroth, J. Anton, X-ray transition energies: new approach to a comprehensive evaluation, Rev. Modern Phys. 75 (2003) 35–99.

[3] G. Buxbaum, G. Pfaff (Eds.), Colored Pigments, John Wiley & Sons, Ltd, 2005, pp. 121–123, (Chapter 3).

[4] C.J. Smith, M.S. Higgs, K.R. Baldwin, The RTO AVT Workshop on 'New Metallic Materials for the Structure of Aging Aircraft', ACM, 1999.

[5] M.J. Scoullos, G.H. Vonkeman, I. Thornton, Z. Makuch, Cadmium, in: M.J. Scoullos (Ed.), Mercury-Cadmium-Lead: Handbook for Sustainable Heavy Metals Policy and Regulation, in: Environment & Policy, vol. 31, Springer, Dordrecht, 2001, pp. 71–272.

[6] H. Morrow, Cadmium and cadmium alloys, in: Kirk-Othmer Encyclopedia of Chemical Technology, American Cancer Society, 2010, pp. 1–36.

[7] S. Velanki, S. Kelly, T. Thundat, D.A. Blake, H.-F. Ji, Detection of Cd(II) using antibody-modified microcantilever sensors, Ultramicroscopy (ISSN: 0304-3991) 107 (12) (2007) 1123–1128.

[8] K. Robbards, P. Worsfold, Cadmium: Toxicology and analysis. A review, Analyst 116 (1991) 549–568.

[9] M. Hutton, Cadmium, in: T.C. Hutchinson, K.M. Meema (Eds.), Lead, Mercury, Cadmium and Arsenic in the Environment, in: SCOPE 31, J. Wiley & sons, Chichester, 1987, pp. 35–41.

[10] L. Blake, S. Mercik, M. Koerschens, K.W. Goulding, S. Stempen, A. Weigel, P.R. Poulton, D.S. Powlson, Potassium content in soil, uptake in plants and the potassium balance in three European long-term field experiments, Plant Soil 216 (1999) 1–14.

[11] J.A. Bearden, X-Ray wavelengths, Rev. Modern Phys. 39 (1967) 78.

[12] Y. Cauchois, C. Sénémaud, Wavelengths of X-ray Emission Lines and Absorption Edges, Pergamon Press, 1978.

[13] S.T. Perkins, D.E. Cullen, M.H. Chen, J.H. Hubbell, J. Rathkopf, J.H. Scofield, Tables and Graphs of Atomic Subshell and Relaxation Data Derived from the LLNL Evaluated Atomic Data Library (EADL), Z=1-100, vol. 30, Lawrence Livermore National Laboratory Report, 1991.

[14] R.F. Egerton, Limits to the spatial, energy and momentum resolution of electron energy-loss spectroscopy, Ultramicroscopy (ISSN: 0304-3991) 107 (8) (2007) 575–586.

[15] J.L. Campbell, T. Papp, Widths of the atomic K-N7 levels, At. Data Nucl. Data Tables 77 (2001) 1–59.

[16] M. Ohno, P. Putila-Mantyla, G. Graeffe, L x-ray linewidths of the elements Nb to Sb II, J. Phys. B: At. Mol. Phys. 17 (1984) 1747–1754.

[17] R. Bonetto, G. Castellano, J. Trincavelli, Optimization of parameters in electron probe microanalysis, X-Ray Spectrom. 30 (2001) 313–319.

[18] A. Sepúlveda, T. Rodríguez, P.D. Pérez, A.P. Bertol, A.C. Carreras, J. Trincavelli, M.A. Vasconcellos, R. Hinrichs, G. Castellano, Structure of the Fe and Ni L X-ray spectra, J. Anal. At. Spectrom. 32 (2017) 385–392.

[19] S. Limandri, J. Trincavelli, R. Bonetto, A. Carreras, Structure of the Pb, Bi, Th, and U *M* x-ray spectra, Phys. Rev. A 78 (2008) 022518 1–10.

[20] J. Trincavelli, G. Castellano, The prediction of thick target electron bremsstrahlung spectra in the 0.25-50 keV energy range, Spectrochim. Acta B 63 (2008) 1–8.

[21] R.D. Bonetto, A.C. Carreras, J.C. Trincavelli, G.E. Castellano, L-shell radiative transition rates by selective synchrotron ionization, J. Phys. B: At. Mol. Phys. 37 (2004) 1477–1488.

[22] T. Rodríguez, A. Sepúlveda, A. Carreras, G. Castellano, J. Trincavelli, Structure of the Ru, Ag and Te L X-ray emission spectra, J. Anal. At. Spectrom. 31 (2016) 780–789.

[23] S. Limandri, R. Bonetto, H. Di Rocco, J. Trincavelli, A suitable expression for the Voigt function. Application to the determination of uranium M linewidths, Spectrochim. Acta B 63 (2008) 962–967.

[24] H. Enkisch, C. Sternemann, M. Paulus, M. Volmer, W. Schülke, $3d$ spectator hole satellites of the Cu $K\beta_{1,3}$ and $K\beta_{2,5}$ emission spectrum, Phys. Rev. A 70 (2004) 022508 1–7.

[25] P.D. Pérez, A.C. Carreras, J.C. Trincavelli, Structure of the sulfur K x-ray emission spectrum: influence of the oxidation state, J. Phys. B: At. Mol. Opt. Phys. 45 (2012) 025004.

[26] F.P. Larkins, Semiempirical Auger-electron energies for elements $10 \leq Z \leq 100$, At. Data Nucl. Data Tables 20 (1977) 311–387.

[27] J.A. Bearden, A.F. Burr, Reevaluation of X-Ray atomic energy levels, Rev. Modern Phys. 39 (1967) 125–142.